Section III. Gaseous detectors

TEST OF A HIGH RESOLUTION DRIFT CHAMBER PROTOTYPE

V. COMMICHAU, M. DEUTSCHMANN, K.J. DRAHEIM, P. FRITZE, K. HANGARTER,
P. HAWELKA, U. HERTEN, D. LINNHÖFER and M. TONUTTI

Rhein.-Westf. Technische Hochschule, III. Physikalisches Institut, Physikzentrum, D-5100 Aachen, Federal Republic of Germany

U. BIERMANN, E. RODERBURG and A.H. WALENTA

Univ. Gesamthochschule Siegen, Fachbereich 7 – Physik, D-5900 Siegen, Federal Republic of Germany

H. ANDERHUB, J. FEHLMANN, H. HOFER, M. KLEIN *, J.A. PARADISO **,
J. SCHREIBER * and G. VIERTEL

Eidg. Technische Hochschule, Institut für Hochenergiephysik, CH-8093 Zürich, Switzerland

The performance of a drift chamber prototype for a colliding beam vertex detector in a test beam at DESY is described. At one (two) atmosphere gas pressure a spatial resolution of 40 μm (30 μm) per wire for one cm drift length was achieved with a 100 MHz Flash-ADC system. An excellent double track resolution of better than 300 μm over the full drift length of 5 cm can be estimated.

1. Introduction

For the identification of short lived particles and the measurement of their lifetime by detection of their decay vertex a position resolution of the tracking devices of $\Delta x < 30$ μm and a double track resolution of $\Delta x < 0.5$ mm will be necessary.

Silicon-strip detectors are ruled out because of multiple scattering and other technical reasons and one is left with drift chambers. A number of such detectors have been installed recently in experiments at e^+e^--machines (MARK II Detector, see e.g. ref. [1]) but the achievable resolution hovers around $\sigma \sim 100$ μm, still a factor of three off from our design goal.

An improvement of this order can only be achieved by fundamental improvements in the detection principle. Therefore this paper contains the description of a track detector based on the "time expansion chamber" (TEC) [2].

In order to describe the basic features of this detector the limiations of position resolution in drift chambers are briefly reviewed [3].
(1) Physical limitations:
   – range of δ-rays,
   – diffusion.

* Visitor from Akademie der Wissenschaften, Institut für Hochenergiephysik, DDR-1615 Zeuthen, German Dem. Rep.
** Now at Draper Laboratory, Cambridge, Mass., USA.

(2) Technical limitations:
   – measurement of cluster position in 3-dimensional space by projection on one coordinate (cluster effect),
   – field line distortions,
   – mechanical precision.

The contribution from the range of δ-rays can be estimated $\sigma < 20$ μm and will be excluded from further discussions. The diffusion is given by $\sigma^2/x = 2\epsilon_k/E$ with x the drift length, E the electrical field strength and ϵ_k the characteristic energy of the electrons.

In standard drift chambers the requirement of "saturated" drift velocity imposes the condition $\epsilon_k \approx 0.3$ eV resulting in $\sigma/x^{1/2} \sim 250$ μm/cm$^{1/2}$ for typical operation conditions. In TEC chambers a "cool" gas is used giving a low drift velocity $v_D \propto E/p$ and resulting in low diffusion of $\alpha/x^{1/2} \sim 100$ μm/cm$^{1/2}$.

The effect of the diffusion can be reduced further, if instead of measuring the arrival of the first electron (leading edge discrimination) the centroid of the essentially gaussian electron cloud of n electrons can be measured. Then one obtains ideally

$$\sigma = \sigma_0/n^{1/2},$$

where σ_0 is the diffusion of a single electron. Due to the slow drift velocity in the drift region of the TEC (fig. 1) and the fast signal formation in the amplification region behind the grid the anode signal reproduces sufficiently well the spatial structure of the arriving electron cloud. Coincidently the electronics industry now offers fast
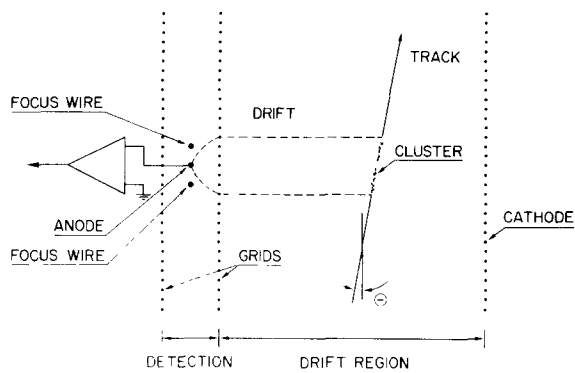
Fig. 1. Principle of construction for a "time expansion chamber".

components such that low cost Flash-ADC's can be developed and successfully operated to permit the centroid measurement on a reasonable large number of wires. The deformation of the arriving electron cloud by the converging field lines in the amplification region can be reduced in the TEC by designing a narrow amplification zone. Due to the considerable reduction of all other contributions this effect emerges now as one of the major limitations but does not endanger the design goal for the position resolution at the current level.

In the TEC vertex detector a high double track resolution will be achieved, limited by diffusion because the anode signal after appropriate shaping reproduces the spatial extension of the arriving electrons from ionization.

Finally a very precise mechanical construction is needed to guarantee a homogeneous drift field. This minimizes off-line corrections, which are more important at low drift velocities than at saturated ones.

2. TEC prototype test

2.1. Drift chamber and gas system

The test chamber is shown schematically in fig. 2. The gas amplification or detection gap is 4 mm wide, i.e. on both sides of the anode wire plane (10 active anodes in total with 10 mm distance between adjacent anode wires) there are wire grids (50 μm wires, 250 μm wide meshes) at 2 mm distance from the anodes. Beyond the two grids extend the 50 mm deep drift regions. To maintain high stability, all grids are held by 18 mm thick stainless steel frames. Fig. 3 shows the space around one anode wire in detail. To the left and to the right there are focus wires to adjust the length of a track segment sampled by the anode. Fig. 4 shows the com-
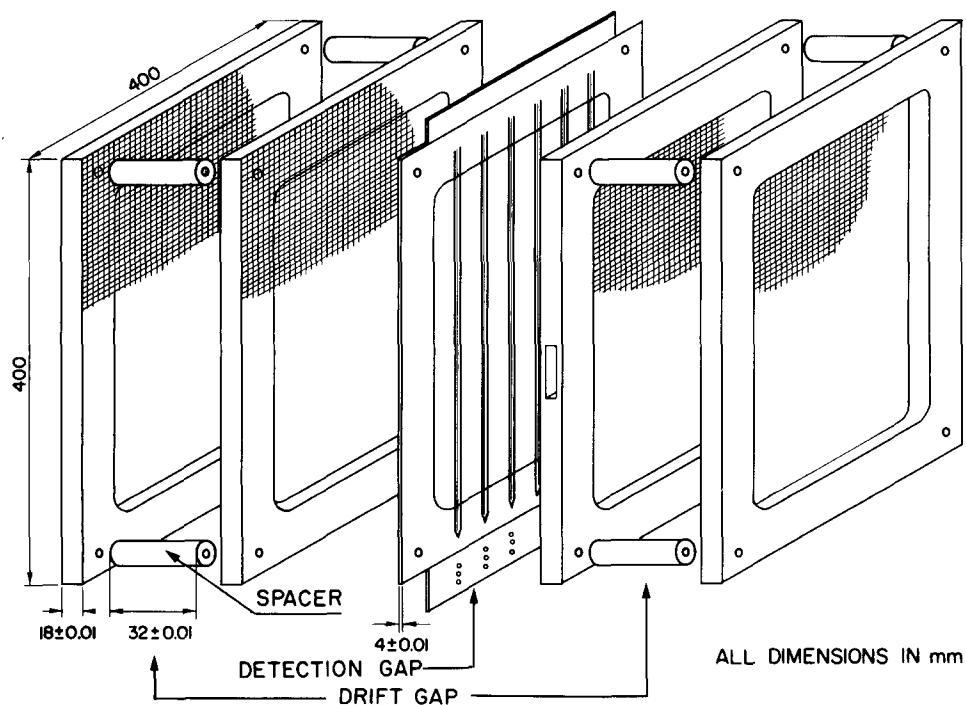

Fig. 2. Exploded view of the test chamber.
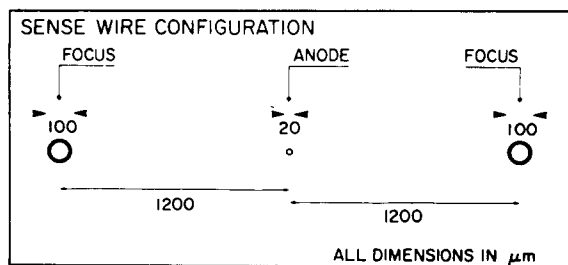
SENSE WIRE CONFIGURATION

Fig. 3. Sense wire configuration.

puted drift paths ending at the anode or at the focus wires respectively. The whole chamber sits inside a rigid aluminium box with beam entrance windows (180 μm mylar).

The chamber has been filled with a CO_2 (80%)/i-C_4H_{10}(20%) gas mixture allowing for thermal electrons (lowest possible diffusion) at an unsaturated drift velocity of 5 μm/ns. In fig. 5 measurements [5] and calculations [6] of the drift velocity and diffusion are shown.

As electron capture in CO_2 strongly depends on very small contaminations by oxygen [7] a closed loop gas system was used, including a deoxo purifier and a mole sieve. In addition an "Oxisorb" purifier was installed at the gas entrance to the chamber, to avoid impurities introduced by diffusion of air through the long (30 m) plastic tubes connecting the gas system with the drift chamber. The gas composition was periodically checked by means of a gas chromatograph.

2.2. Electronics and data aquisition

The preamplifiers [8] for the sense wires consist of two stage units (fig. 6). The first stages are kept inside the chamber box near to the wires. Through short twisted pair cables they are connected to the second stage amplifiers outside of the box, which drive 50 Ω cables to the counting room. The rise time of the combined preamplifiers is about 3 ns and the noise corresponds to 2000 electrons rms over the full bandwidth.

The pulses arriving at the counting room are fed to shapers [8] of the type described by Boie et al. [4]. A circuit diagram is shown in fig. 7. The shapers accept either polarity up to about 300 mV with an output driving over ±1 V into a 50 Ω load. Every shaper output is fanned out to a 1 ns TDC and to a CAMAC based 100 MHz 6 bit Flash-ADC, loading in 10 ns time bins a 1024 word deep 6 bit ECL memory, i.e. sampling over a total span of 10.24 μs. The FADC's are built around TRW 1029 digitizers, having a large bandwidth (150 MHz) [9].

All FADC's are run on a common external clock. To increase the time resolution, the trigger pulse delayed by a fixed time span (9.200 μs) is fed to one of the detection gap grids to make it appear as a reference pulse at the end of all FADC readings. The precision of this time reference measurement has been checked. A jitter of 240 ps is inferred from the plot in fig. 8. As an example of the FADC readings the digitization of a single track (left hand side) on all 10 anode wires is
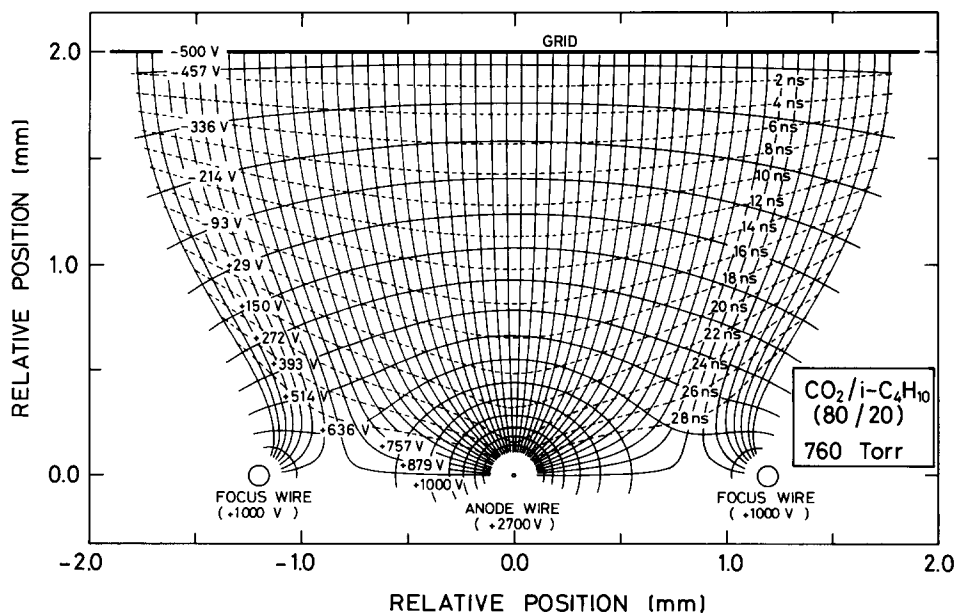

Fig. 4. Computed isochronous lines, field lines and potential lines in the detection gap at the sense wire configuration.
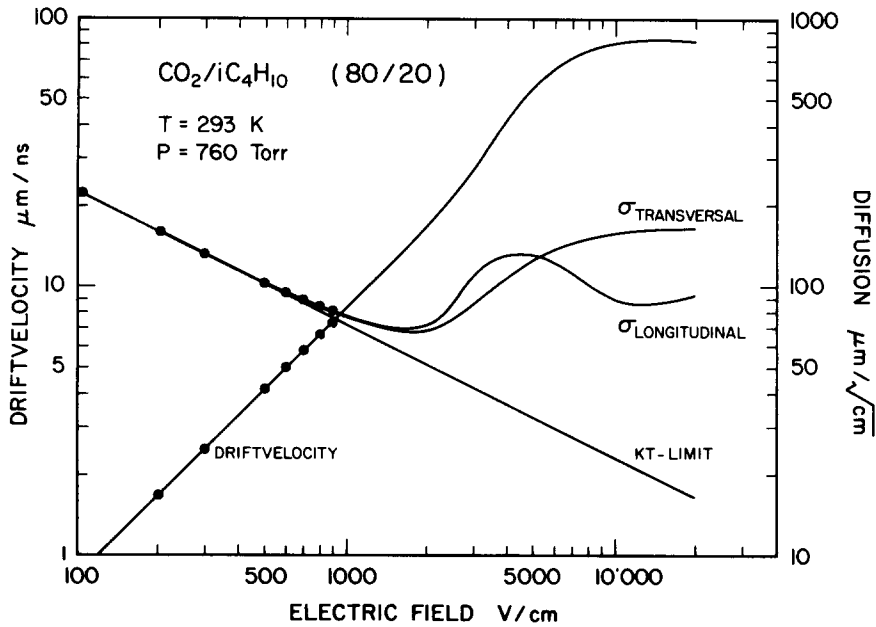
Fig. 5. Calculations (full lines) and measurements (points) of the drift velocity and diffusion of the gas mixture used.
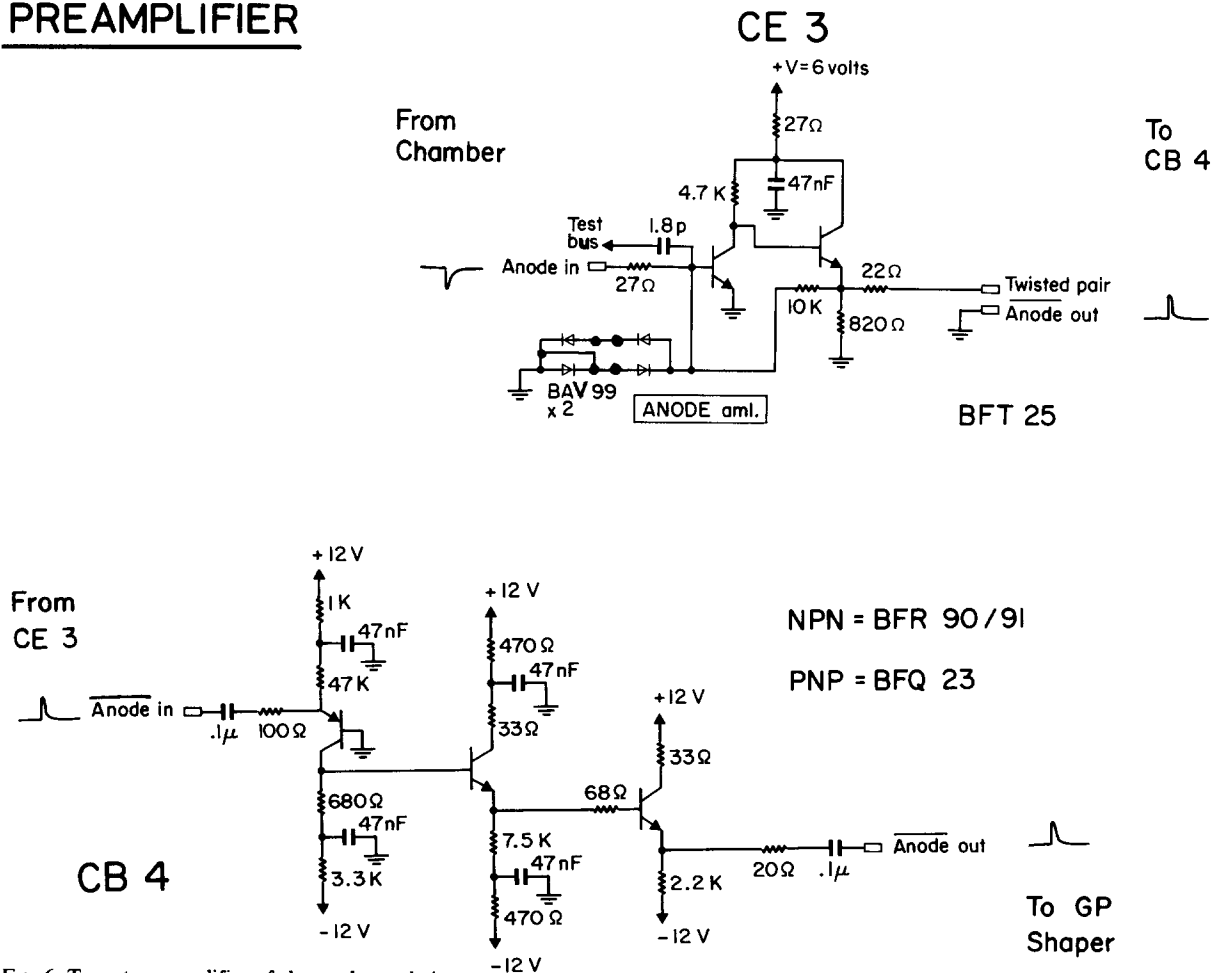
PREAMPLIFIER

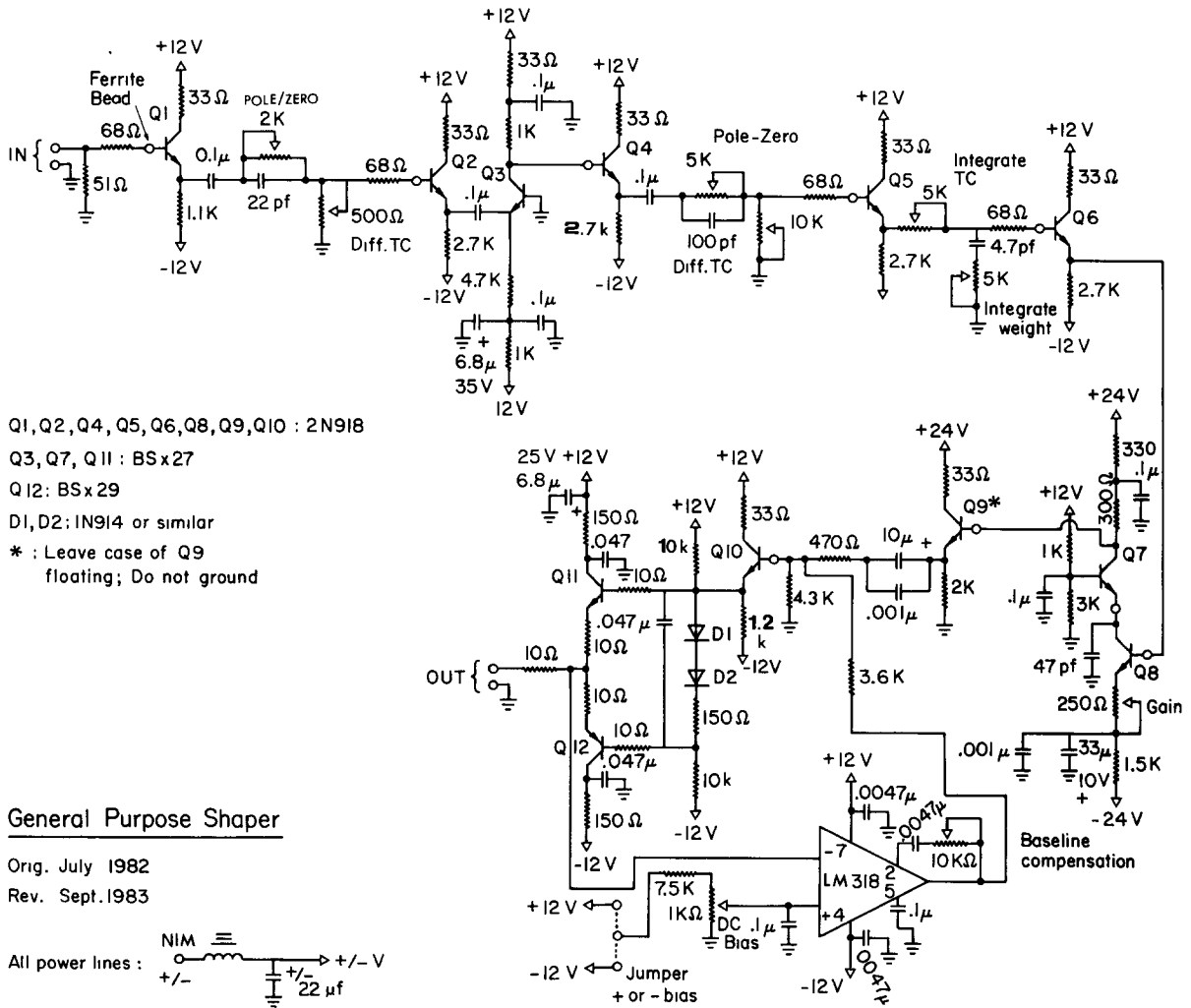Fig. 6. Two stage amplifier of the read out chain.

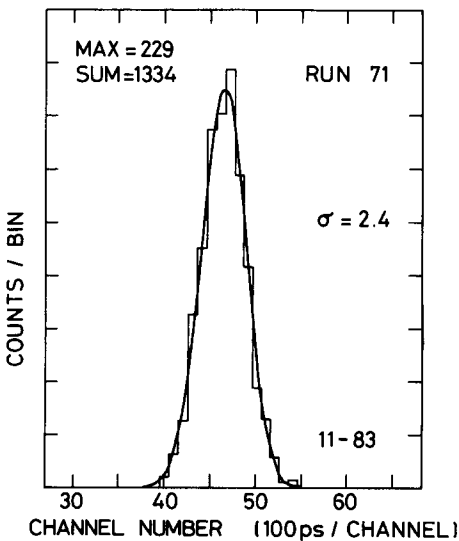Fig. 7. Schematic of the general purpose shaper.

Fig. 8. Center of gravity time jitter of the time reference signal.

shown in fig. 9, together with the corresponding drift length scale. The reference pulses appear to the extreme right (for analysis the center of gravity of the first peak only is taken). Track data, but on an expanded time scale are displayed in fig. 10.

The experiment was controlled by an interactive program running on a PDP 11/40, which read the CAMAC devices, did some on-line checking and wrote the events on magtape.

2.3. The test set-up

The test was performed at DESY with an electron beam of 4 GeV/c momentum and with a set-up as shown in fig. 11. The trigger was generated by a coincidence of the scintillation counters Z1, Z2 and Z3. The beam thus defined had a width of about 4 mm. To cover the full depth of the drift space, the test chamber could be moved in well defined (10 μm) steps perpendicular to the beam direction. Fig. 12 shows the measured beam

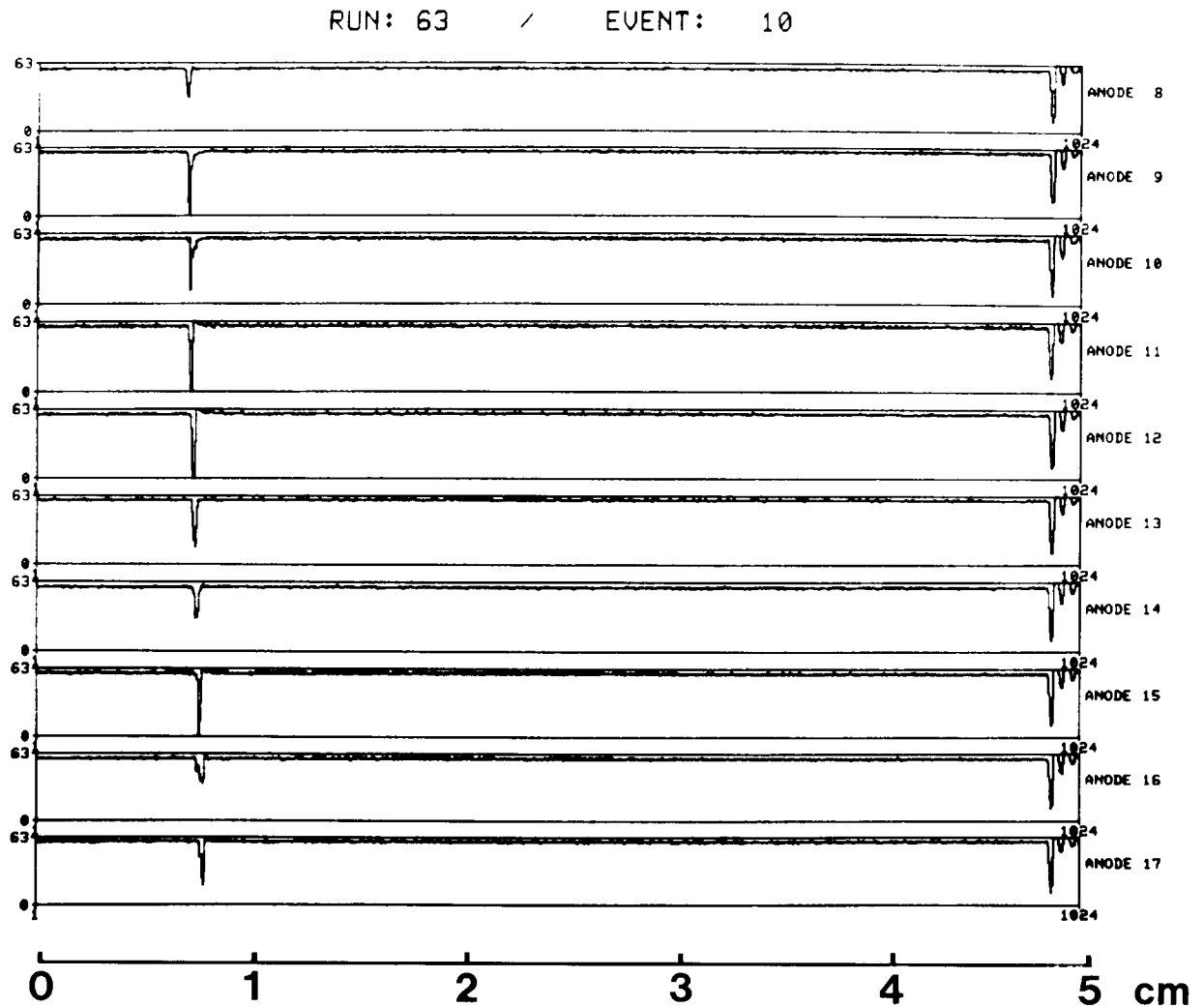III. GASEOUS DETECTORS

RUN: 63   /   EVENT: 10

Fig. 9. Display of the 10 FADC data recorded on tape. Also shown is the corresponding scale of the drift length.

profiles for 5 different positions of the chamber (For the first position near the grid the beam passed through a hole in the chamber frame to be seen in fig. 2.) For

Table 1
Measured drift velocities

Drift field (kV/cm)	Pressure (bar)	Drift length (mm)	Drift velocity (μm/ns)
		13.5 ± 7	6.06 ± 0.12
0.70	1	27.5 ± 7	5.99 ± 0.08
		38.0 ± 3.5	6.11 ± 0.18
		13.5 ± 7	4.80 ± 0.08
		24.0 ± 3.5	4.68 ± 0.14
1.10	2	31.0 ± 3.5	4.80 ± 0.16
		38.0 ± 3.5	4.80 ± 0.19

precise knowledge of the beam position three fixed position drift chambers CH1, CH2 and CH3, read out by TDC's were placed up stream of the test chamber.

To get high space resolution the drift velocity has to be constant and known with high precision. It was determined from the differences in the drift time at several well defined beam positions in the chamber, which were fixed by very narrow time windows in the above mentioned chambers CH1 through CH3. Table 1 shows the results for different parts of the runs at gas pressures of 1 and 2 atm. Within errors no dependence of the drift velocity on the drift path is seen.

2.4. Flash-ADC data analysis procedure

The main steps of the data analysis are shown in fig. 13. The raw data consist of a pulse train stored in the
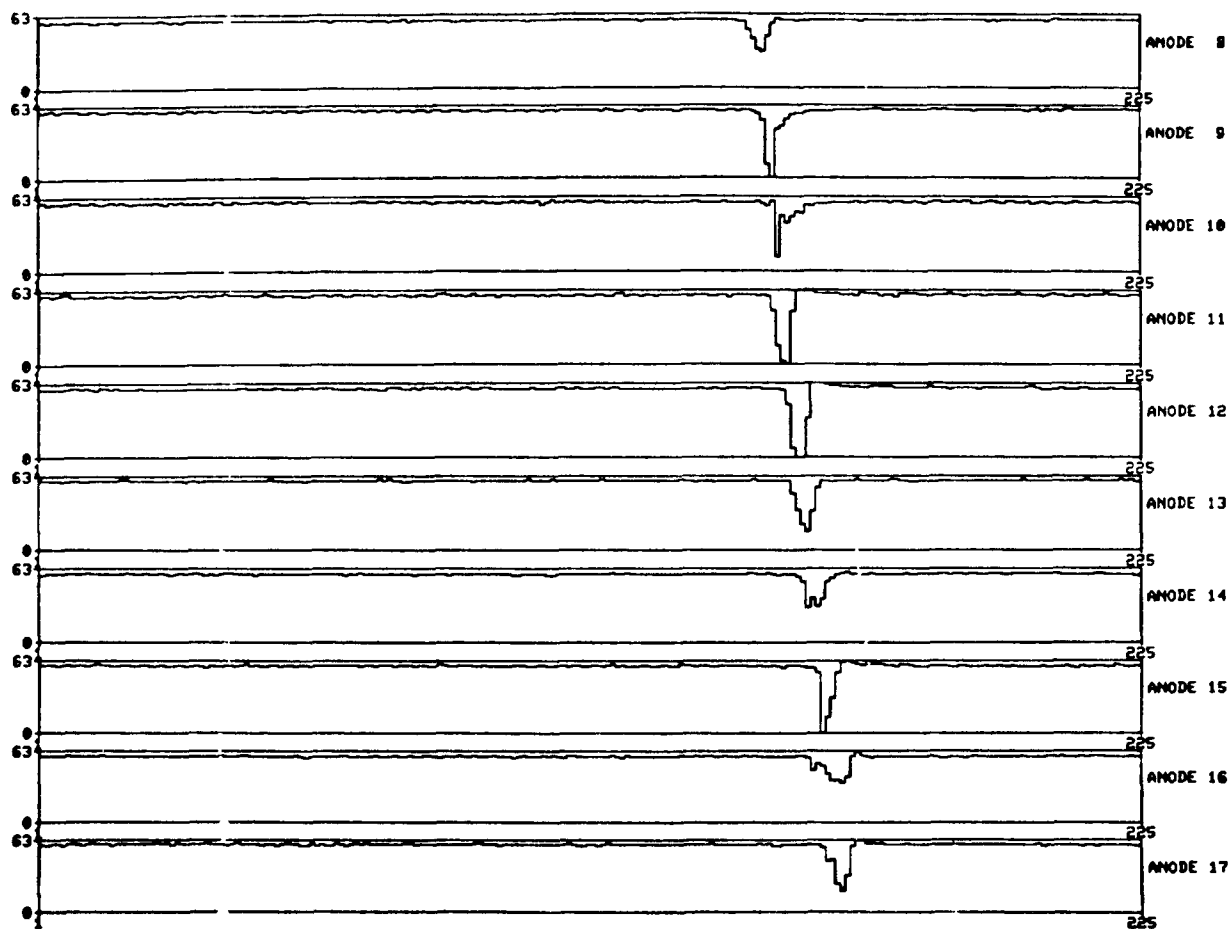
RUN: 63 / EVENT: 10

Fig. 10. Expanded display of the FADC raw data.

1024 FADC channels. The base line heights for the time marker is determined from the mean contents of channel 700 to 990 of the FADC. For all other pulses a global base line is calculated from channels 10 to 350.

The pulse position is found by the following procedure (fig. 14):

A threshold (T) is applied (3 counts above the base line) and every signal crossing the threshold, being of a
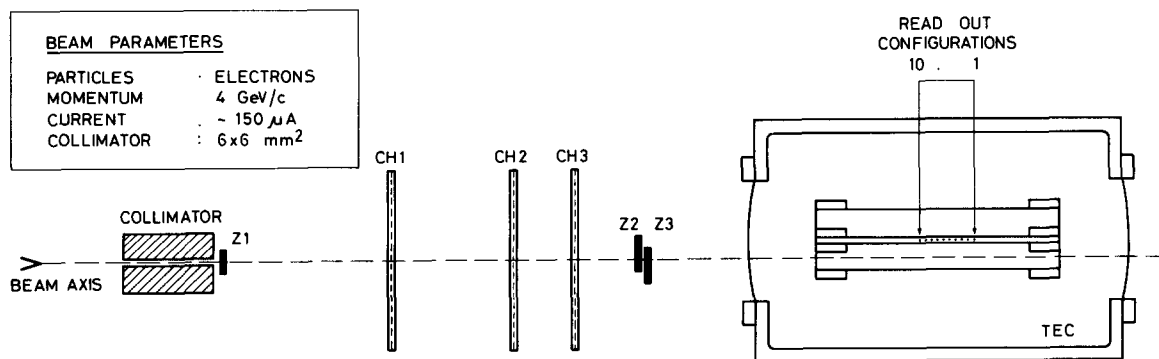

Fig. 11. Test set-up used in the DESY electron beam.
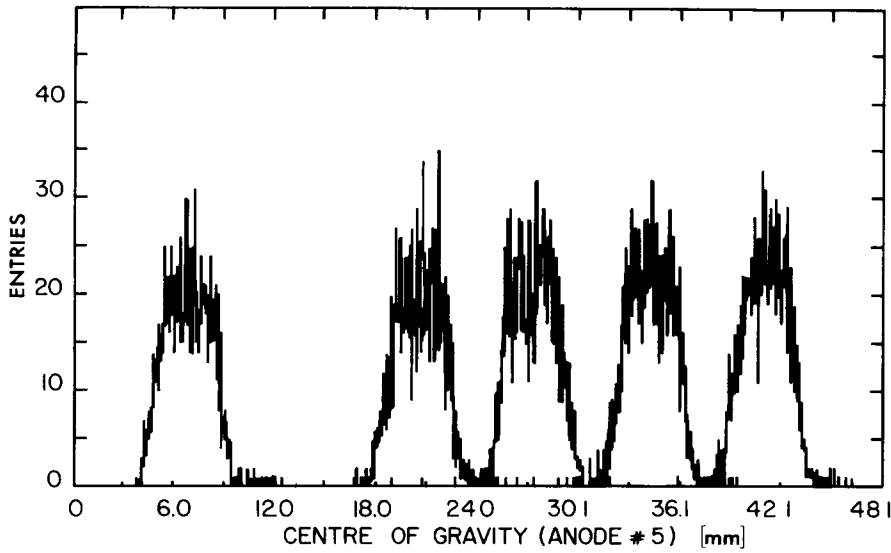
BEAM PROFIL RUN 68 - 72 ANODE 5

Fig. 12. Beam profile measured for different drift lengths.

width L or wider with at least a distance P to the next one, is considered as one peak (standard setting: $L = 2$ channels, $P = 10$ channels). Let b and e be the channel numbers, where the signal of one peak crosses the threshold the first time (b) and the last time (e). Then the center of gravity for the channels (b) through (e) is calculated:

$$T = \sum_{i=b}^{e} \max[(C_i - B), 0] t_i / \sum_{i=b}^{e} \max[(C_i - B), 0]$$

with C_i being the channel content, B the base line, $\max[(C_i - B), 0]$ the signal above base-line, but not negative, t_i the channel number and T the pulse position.

A least squares fit for a straight line for all the times T_j determined (anode numbers $j = 1, \ldots, 10$) is performed subsequently and the fitted times F_j are calculated. To take into account the differing weights of the anodes caused by geometry, the time residua

$$r_j = T_j - F_j \quad (j = 1, \ldots, 10)$$

are multiplied by a weight factor g_j

$$g_j = N \left\{ \sum_{k=1}^{10} \left[a_k \left(\langle x^2 \rangle - \langle x \rangle (x_k + x_j) + n x_k x_j \right) \right. \right.$$
$$\left. \left. - \delta_{jk} N \right]^2 \right\}^{-1/2} ,$$

RAW DATA

C.O.G. OF TIME MARKERS
C.O.G. OF SIGNALS
INTEGRAL OF SIGNALS

LINE FIT

RESIDUUM FOR ALL
ANODES

RESIDUUM FIT
(GAUSS + CONST)

RESOLUTION
(MEAN OVER ALL ANODES)

FIT X-DEPEN
$(\sigma = \sqrt{A^2 x + B^2})$

Fig. 13. Data analysis procedure.

S . SEARCH RANGE WITHIN CHANNEL I TO 1023
B . BASELINE
T   THRESHOLD
P . MINIMUM NUMBER OF CHANNELS TO SEPARATE TWO PEAKS
L: MINIMUM NUMBER OF CHANNELS OVER THRESHOLD TO BE A PEAK
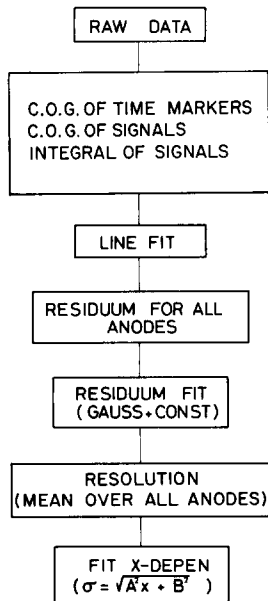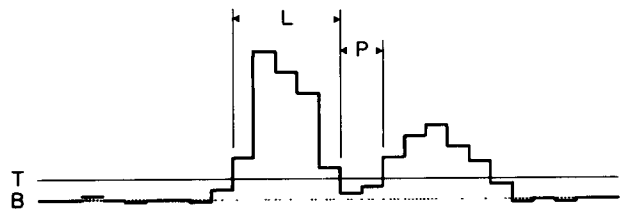M: MAXIMUM NUMBER OF PEAKS ALLOWED

Fig. 14. Data analysis parameter list.
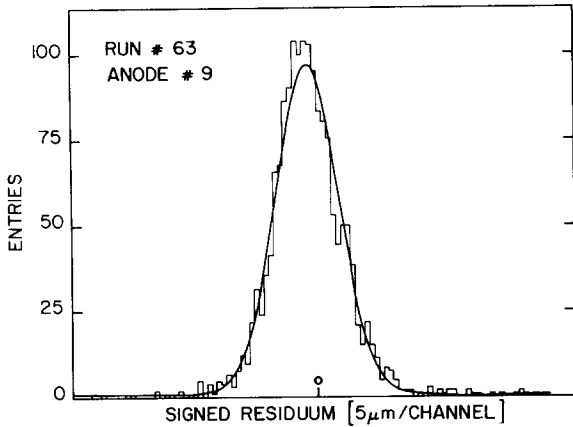
Fig. 15. Single wire residua distribution measured at a gas pressure of two atmospheres and a mean drift length of 7 mm.

$$N = n\langle x^2 \rangle - \langle x \rangle^2,$$

n = number of anodes in the fit,

x_l = position of the anode number l in the beam direction,

a_h = 1 (0), if the anode number h is used (not used) in the fit,

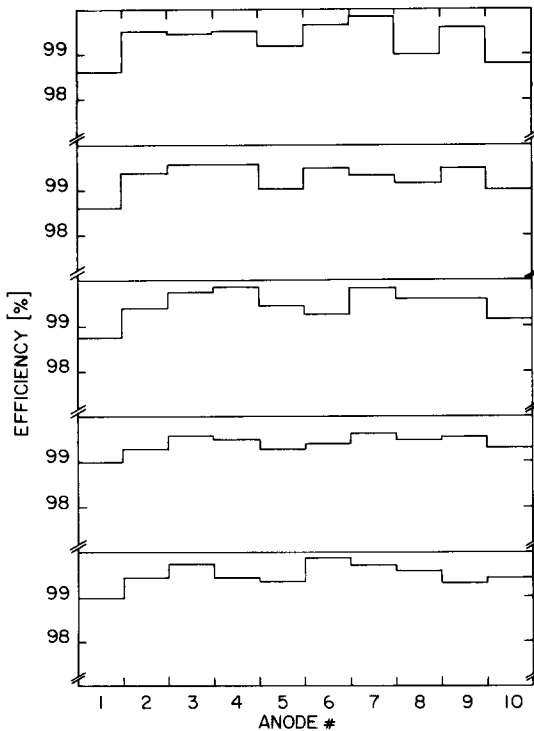$$\langle x \rangle = \sum_{l=1}^{10} a_l x_l.$$

Fig. 16. Anode analysis efficiency.

The assumption is made that the resolution of all anodes is the same. The quantity which is plotted in fig. 15 is the weighted space residual

$$R_j = r_j g_j v_D \quad (j = 9)$$

with the drift velocity v_D.

To this distribution a gaussian curve with constant "background" is fitted. The gaussian width σ_j is the resolution of the anode number j. The resolution of the chamber is the mean value of the σ_j's of all anodes. This chamber resolution was determined for different distances x of tracks with respect to the detection grid. Under the assumption that a fraction of the resolution $\sigma(x)$ is due to the longitudinal diffusion (A) and the remaining part (B) is independent of drift distance, a fit with a function

$$\sigma(x) = (A^2 x + B^2)^{1/2}$$

is applied.

2.5. Results

The results presented are restricted to measurements with clean single tracks ($> 90\%$ of the total sample) nearly parallel (0.8°) to the read out plane. Fig. 16 shows the anode analysis efficiency for the run at 2 atm gas pressure at different drift lengths (For a standard set of parameters (fig. 14): $T = 4$, $P = 10$, $L = 2$, $M = 1$.) The inefficiency observed is mainly due to a too small signal height as found by inspection of the raw data displays.

In fig. 17 the mean pulse width (2 atm run) is shown as a function of the drift length. A fit through the measured values with a function

$$W = (C^2 + xD^2)^{1/2}$$

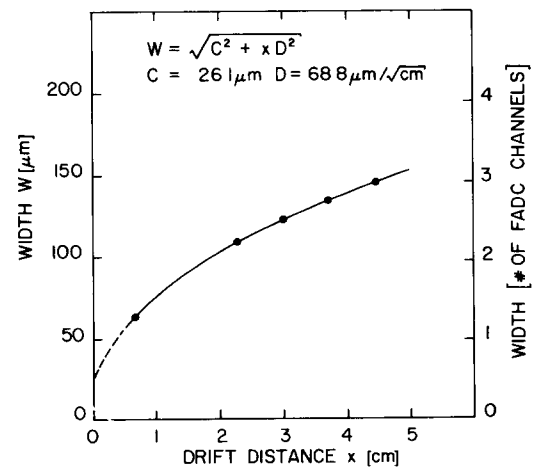delivers $C = 26.1$ μm and $D = 68.8$ μm/cm$^{1/2}$. D corre-

Fig. 17. Mean pulse width versus drift distance.

Table 2
Measured single wire resolution

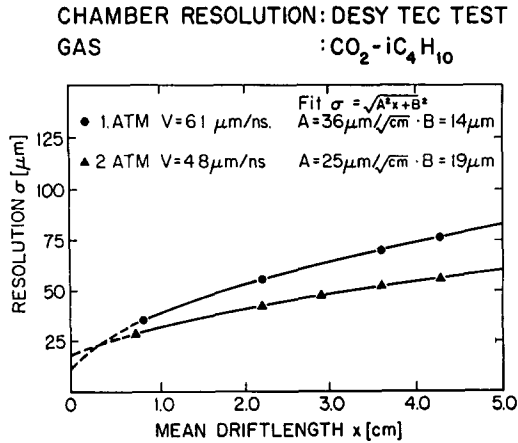| Pressure (bar)	Spatial resolution $\sigma(X)$ in μm mean drift length X					
	$X = 7$ mm	$X = 8$ mm	$X = 22$ mm	$X = 29$ mm	$X = 36$ mm	$X = 43$ mm
1	–	35	56	–	70	76
2	28	–	43	48	51	55

Fig. 18. Measured spatial resolution of the chamber at one and two atmospheres (FADC read out).

sponds to the longitudinal diffusion and is in perfect agreement with previous measurements and calculations (see fig. 5) at one atmosphere pressure, when corrected

for the pressure (70 μm/cm)$^{1/2}$. Term C accounts for the intrinsic width of the electronics, which was measured to be about 6 ns, again in good agreement with C divided by the drift velocity of 4.8 μm/ns ($C/v_D = 5.4$ ns).

Following the analysis procedure described in the previous section the chamber resolution was determined at one and two atmospheres gas pressure (fig. 18) from the FADC data (see also table 2). Simultaneously, i.e. for the same events, the leading edges of the signals were recorded with the TDC's for the 2 atm runs. One observes on average a 20–40% improvement of $\sigma(x)$ with the center of gravity, as compared to the simpler leading edge method, where the stronger reduction is found for longer drift paths (fig. 19). This latter finding is explained by the fact that the spread of the ionization structure due to longitudinal diffusion has less influence on the center of gravity than on the leading edge.

The points in fig. 18 are fitted by the expression

$$\sigma(x) = \left(A^2 x + B^2\right)^{1/2},$$

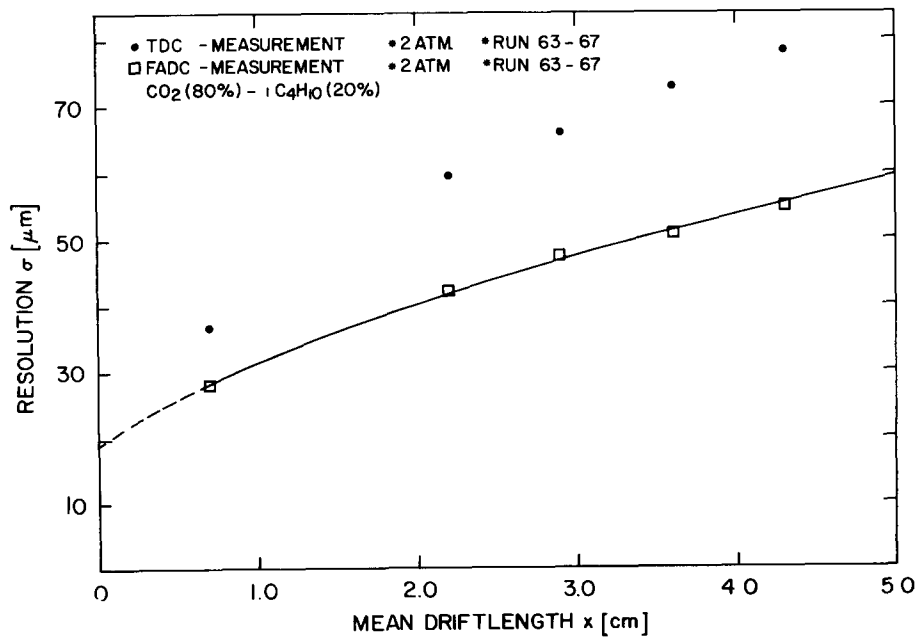in which A represents the contribution from the longi-

Fig. 19. Results for the chamber resolution measured simultaneously by a TDC and FADC system.
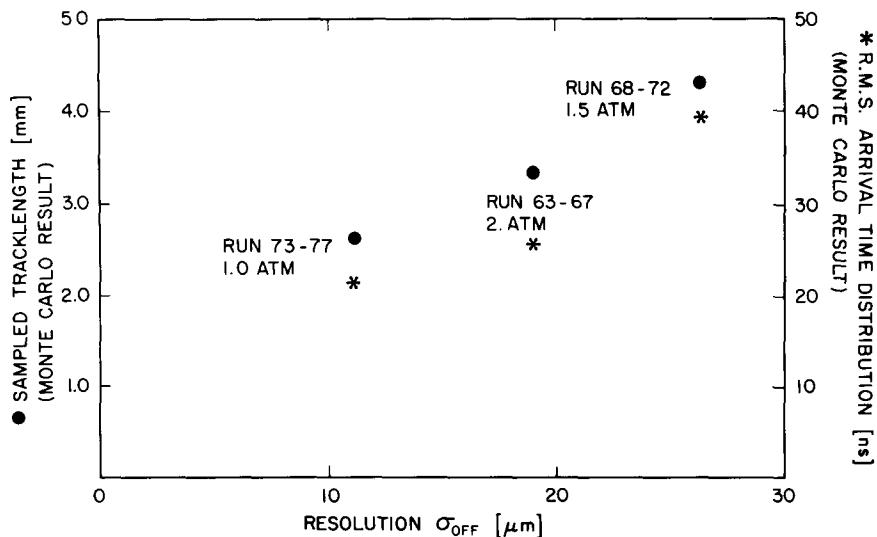
Fig. 20. The extrapolated chamber resolution at zero drift length $x = 0$ (resulting from a fit $\sigma = (Ax^2 + \sigma_{OFF}^2)^{1/2}$ to the experimental data) as a function of the computed sampled track length (left scale) and rms of the arrival time distribution of the drift electrons at the anode (right scale). For the Monte Carlo calculation the different settings of the high voltages and the gas pressure for the three sets of runs were taken into account.
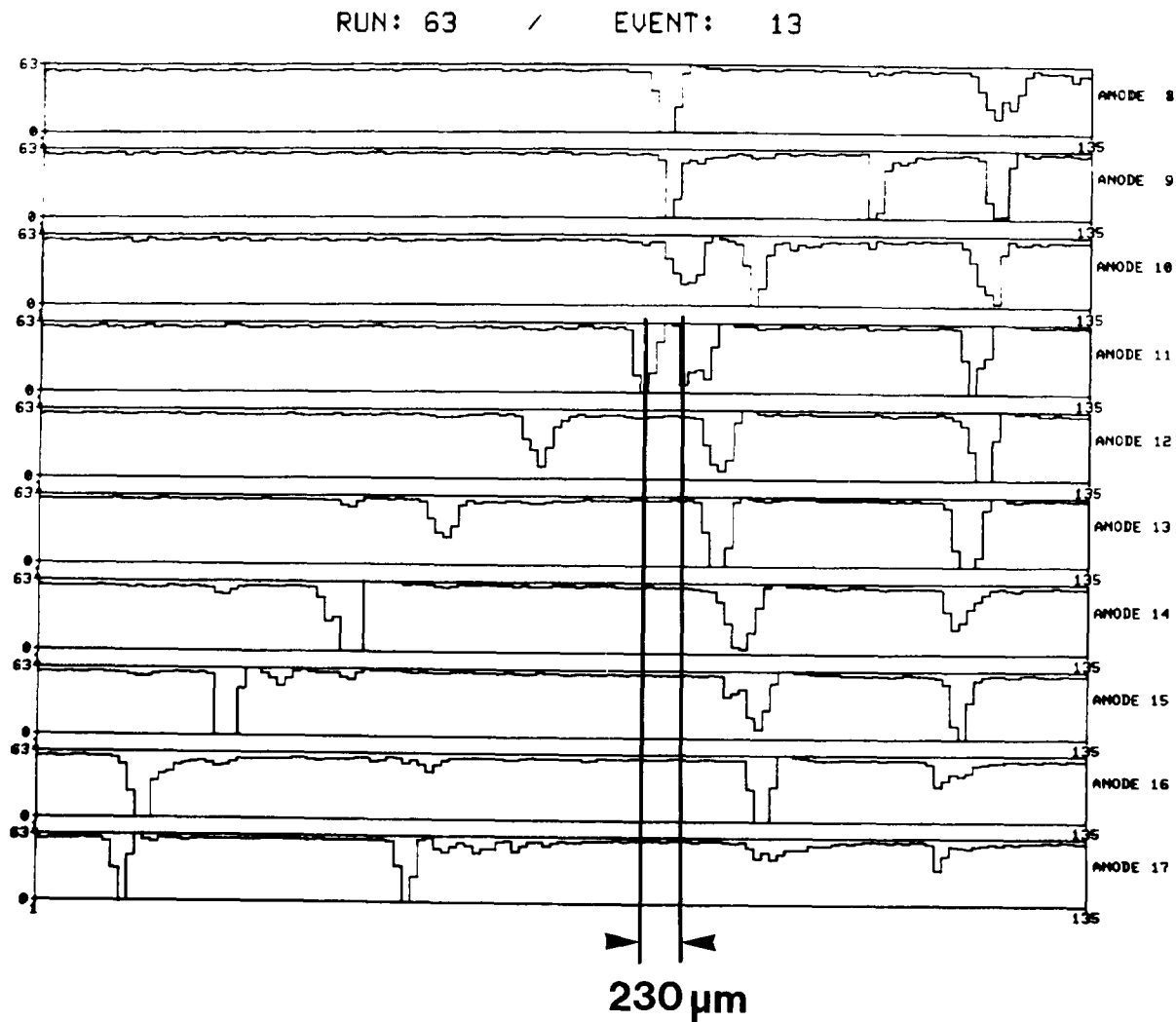
RUN: 63 / EVENT: 13

Fig. 21. Expanded display of the raw data for a multi track event.

tudinal diffusion, whereas B is independent of drift length and due to mechanical precision, electronic resolution and fluctuations of the ionization along the track. It especially depends on the width of the arrival time distribution of the electrons on the sense wire, or in other terms the sampled track length. This is clearly proven in fig. 20, where a strong dependence of the extrapolated chamber resolution $\sigma(0) = B$ from the sampled track length for different running conditions is demonstrated.

The excellent double track resolution which is achieved by a FADC read out can be derived from the mean pulse width as a function of drift length in fig. 17 and is visually demonstrated in fig. 21. A double track resolution of 300 μm over the full drift length for small angle tracks can be estimated.

3. Conclusion

For drift lengths less than 5 mm, spatial resolutions achieved with TDC's are comparable to those with FADC's. For longer drift paths, however, the FADC read out becomes superior and in addition provides excellent multi track resolution. If the tight tolerances in a mechanical layout for a larger drift chamber can be kept, a mean spatial resolution of 30 μm for a single wire at one cm drift length in an experimental set-up can be expected.

References

[1] J. Jaros, Proc. Int. Conf. on Instr. for Colliding Beam Phys., February 1982, SLAC-250, UC-34d; B. Foster, Tasso Collaboration, Int. Conf. on HE Physics, Brighton (July 1983).

[2] A.H. Walenta, IEEE Nucl. Sci. NS-26, Nr. 1(79) 73; J. Fehlmann, H. Hofer, J. Paradiso, G. Viertel and A.H. Walenta, Proc. Int. Conf. on Instr. for Colliding Beam Phys., Stanford 1982, SLAC-25, UC-34d.

[3] A.H. Walenta, IEEE Trans. Nucl. Sci. NS-22 (1975); F. Sauli, Nucl. Instr. and Meth. 156 (78) 147; A.H. Walenta, Review of the Physics and Technology of Charged Particle Detectors, 1983 SLAC Summer Inst., preprintSi-83-23, Siegen 1983; G. Charpak and F. Sauli, CERN-EP/84-35, submitted to Ann. Rev. Nucl. Sci.

[4] R.A. Boie, A.T. Hrisoho and P. Rehak, IEEE-NS 28 (1981) 603.

[5] P. Binet, Diploma work, ETH Zürich (1984).

[6] J. Fehlmann, J.A. Paradiso and G. Viertel, "WIRCHA" a program package to simulate drift chambers, ETH Zurich (1983).

[7] J.L. Pack and A.V. Phelps, J. Chem. Phys. 45 (1966) 4316.

[8] J.A. Paradiso, Compilation of Data on the Current TEC Analog Electronics, ETH Zürich (1983).

[9] V. Commichau, Internal Report, III. Phys. Inst. RWTH Aachen (1984).